Accepted Manuscript

Thermo- and cathodoluminescence properties of lepidolite

Y. Rodríguez-Lazcano, V. Correcher, J. Garcia-Guinea

PII: S1386-1425(13)00456-3
DOI: http://dx.doi.org/10.1016/j.saa.2013.04.107
Reference: SAA 10498

To appear in: *Spectrochimica Acta Part A: Molecular and Biomolecular Spectroscopy*

Received Date: 24 January 2013
Revised Date: 18 April 2013
Accepted Date: 24 April 2013

Please cite this article as: Y. Rodríguez-Lazcano, V. Correcher, J. Garcia-Guinea, Thermo- and cathodoluminescence properties of lepidolite, *Spectrochimica Acta Part A: Molecular and Biomolecular Spectroscopy* (2013), doi: http://dx.doi.org/10.1016/j.saa.2013.04.107

Thermo- and cathodoluminescence properties of lepidolite

Y. Rodríguez-Lazcano[(1)], V. Correcher[(2)], J. Garcia-Guinea[(3)]

[(1)]CSIC. Instituto de Estructura de la Materia, Serrano 121, Madrid 28006, Spain.

[(2)]CIEMAT. Av. Complutense 22, Madrid 28040, Spain.

[(3)]CSIC. Museo Nacional Ciencias Naturales, José Gutiérrez Abascal 2, Madrid 28006, Spain.

Abstract

Lepidolite, $K(Li,Al)_3(Si,Al)_4O_{10}(F,OH)_2$, and many of the related phyllosilicate mineral of the mica group have been well studied from the chemical and structural point of view; however, to the best of our knowledge, studies on their luminescence properties have been scarcely reported. This work focuses on the thermoluminescence (TL) and cathodoluminescence (CL) response of a natural lepidolite from Portugal previously characterized by means of environmental scanning electron microscope (ESEM) and X-ray fluorescence (XRF) and atomic absorption spectroscopy (AAS) techniques. The complexity of the thermoluminescence glow curves of non-irradiated and 1Gy irradiated samples suggests a structure of a continuous trap distribution involving multiorder kinetics. UV-IR CL spectral emission shows seven peaks centered at 330, 397, 441, 489, 563, 700 and 769 nm. Such emission bands could be due to (i) structural defects, i. e. $[AlO_4]$ or non-bridging oxygen hole centers, and (ii) the presence of point defects associated with Mn^{2+} and Fe^{3+}.

Keywords: lepidolite, thermoluminescence, cathodoluminescence

Corresponding author: Y. Rodriguez-Lazcano, Instituto de Estructura de la Materia – CSIC, Serrano 121, 28006 Madrid SPAIN. E-mail: fermi2000@yahoo.com

1. Introduction

Lepidolite, $K(Li,Al)_3(Si,Al)_4O_{10}(F,OH)_2$, is a secondary source of lithium and is one of the major sources of rubidium and cesium elements. Besides the well known application of lithium compounds in dosimetry (TLD-100 [1], Gr-200 [2]), ^6Li is used as raw material for tritium production and as a neutron absorber in nuclear fusion [3]. Additionally, lithium minerals are employed in batteries [4] and in the manufacture of glass [4] and ceramics [5]; among others. This is a phyllosilicate mineral of the mica group showing complex variable compositions because of the tendency for isovalent and heterovalent isomorphism substitutions to form series with muscovite and other Li-rich micas such as zinnwaldite [6]. It appears in granite pegmatites, in some high-temperature quartz veins, greissens, and granites. Lepidolite, like other micas, has a layered structure of lithium aluminum silicate sheets weakly bonded together by layers of potassium ions, where all the three octahedral sites are occupied by the cations. The composition depends on their relative amounts of Al and Li in octahedral coordination where, additionally, monovalent cations (mainly Na, Rb and Cs) can replace K. All of the intrinsic (i.e. lattice defects) and/or extrinsic (i.e. impurities) defects as well as structural defects and their distribution in the lattice are responsible for the luminescence emission that is commonly observed in insulator materials during excitation with temperature, electrons, ions, UV or ionizing radiation. In fact, luminescence techniques, e.g., thermoluminescence (TL), cathodoluminescence (CL), optically stimulated luminescence (OSL) and radioluminescence (RL), are usually employed not only for dosimetric purposes (dating, retrospective dosimetry or radiological terrorism), but also for material characterisation. Both TL and CL provides information about the trapped charge recombination sites related to metastable defects inside the lattice depending on whether the detrapping process is due to heat or electron exposure, respectively. All factors involved in the luminescence phenomena (i.e. lifetime, efficiency, emission spectra, etc.) depend directly on the crystalline phase, which is mainly influenced by pressure and temperature. Thus, small variations in the lattice structure due to the presence of inclusions, impurities, substituted ions or surface defects in ppm concentrations show changes in the intensity and wavelength position the emission spectra [7]. Information on the trap structure can be obtained by means of initial rise (IR) analysis. It consist in the premise that occupancies of the relevant states remain almost constant for the lowest temperature side of the TL peak and, therefore,

this side of the peak will follow an exponential dependence regardless of the kinetic order [8, 9].

To the best of our knowledge thermoluminescence properties of micas in general (muscovite [10,11], sericite [10] and phlogopite [10]) and lepidolite in particular, have been scarcely studied. Only Kasuya and co-workers [12] analyzed the annealing effects on the sensitivity of gamma-induced thermoluminescence on natural lepidolite mica from Madagascar. This work reports on the study of the CL and TL emission of a natural lepidolite collected from the pegmatite of Mangualde (northern Portugal). The sample has been structural and chemically characterised by means of Impact-S microscope (ESEM), XRF and AAS techniques.

2. Experimental

The natural lilac-pink lepidolite collected from Mangualde (Viseu, Portugal), was examined on an ESEM microscope, of FEI Company, settled in the Spanish National Museum of Natural Sciences (MNCN). It is a low-vacuum ESEM with a large sample chamber wide enough to hold large samples without the sputtered covering onto sample. The chemical composition was determined in the Spanish MNCN Museum by XRF using a PHILIPS PW-1404 spectrometer with a Sc-Mo tube, Ge, LIF220, LIF200, PE and TLAP analyzer crystals and Super-Q manager from Panalytical-Spain as analytical software. For the XRF measurements, lepidolite pellets of 8 g of milled sample with 0.1 g of elbacite were pressed under 20 TM and dried at 40°C in a climatic chamber. The lithium amount was obtained by means of the AAS technique (Perkin Elmer spectrometer Mod. 2380) with an specific AAS intensitron lamp M-705 for the element Li. Nondestructive chemical analyses of major and minor elements were performed by electron microprobe analysis (EMPA) to provide spatially resolved information on the chemical homogeneity. The sample was bound together with a polymer and softly polished, offering a flat surface to the EMPA beam. The crystal-chemical characteristics of the aluminosilicate were determined on data series of electron microprobe analyses (JEOL Superprobe JXA-8900M), bulk and channel selected (TAP, PETJ, LIF, PETH) X-ray spectra search, and by identification routines. The used standards were natural and synthetic crystals from the collection of the “Servicio de Microscopia Electronica Lluis Bru”, Universidad Complutense de Madrid. The ZAF program was used for

correction of matrix effects. The spot diameter of the probe was ca. 5 µm, and the operating conditions were 15 kV and 20 nA. The lithium light element of lepidolite burns under e-beam or X-irradiation, it is unstable to be analyzed by XRF o by EPMA. In addition to the X-Ray Fluorescence Spectrometry method, the total concentration of fluorine element contained in the lepidolite phases was also determined using a Fluoride Ion-Selective Electrode (ELIT 8221) on free fluorine element previously dissolved in water. Lepidolite grinded sample with Na_2CO_3 flux were melted at high temperature (800ºC) into a platinum crucible by acid attack with hydrochloric and nitric acid (1:1). Later, we added a high ionic strength, weakly acidic buffer to the standards and analysis solutions. The used buffer was a total ionic strength adjustment buffer (TISAB) being 1M in both acetic acid and NaCl with pH 5.2 – 5.4 that was necessary to avoid interferences (OH bindings, HF formation, to control the ionic strength, etc). The analytical procedure for using the fluoride electrode consists of preparing a series of fluoride solutions of varying but known concentrations containing TISAB. The standards will be made from a 100 µg/mL F- stock standard solution.

The stability of TL signal has been studied for natural non-irradiated samples (NTL) and 1Gy beta irradiated samples (ITL) using a preheat technique that consists of linear heating of the samples up to a temperature T_{stop} followed by quick cooling to room temperature and final readout to record the whole remaining TL glow curve [13], where thermal preheating varies from 190 to 280ºC. The TL measurements were performed using an automated Risø TL reader model TL DA-12 provided with an EMI 9635 QA photomultiplier [14]. The emission was observed through a blue filter (a FIB002 of the Melles-Griot Company) where the wavelength (in nm) is peaked at 320-480 nm; FWHM is 80±16nm and peak transmittance (minimum) is 60%. The TL reader is also provided with a $^{90}Sr/^{90}Y$ source with a dose rate of 0.021Gy s^{-1} calibrated against a ^{137}Cs photon source in a secondary standard laboratory [15]. The sample was carefully powdered with an agate pestle and mortar to avoid triboluminescence [16]. All the TL measurements were performed using a linear heating rate of 5°C s^{-1} from room temperature up to the corresponding temperature in a N_2 atmosphere. Aliquots of 5.0 ± 0.1 mg of the sample were used for TL measurements.

The CL spectra were measured using a Gatan MonoCL3 detector with a PA-3 photomultiplier tube attached to the ESEM model XLS30. The detector covers a spectral range of 250–850nm and is the most sensitive in the blue parts of the spectrum.

The samples were placed on polished slabs, at low-vacuum mode without coating to keep open way out to the CL emission. The emission of the samples was collected and amplified using a retractable parabolic diamond mirror and a photomultiplier tube. The distance between the sample and the bottom of the CL mirror assembly was 15mm. The excitation for CL measurements was provided at 25 kV electron beam.

3. Results and discussion

An ESEM image of two pieces of the lepidolite sample is shown in Figure 1. The structure is homogeneous and with laminar texture characteristic of the mica. Li-micas, like lepidolite are principally linked to the core margin and the replacements units of the pegmatites. However, book micas are the most homogeneous since they were collected from the intermediate zone of the pegmatite. Micas from core margins or intermediate units of the pegmatites usually exhibit inhomogeneities with different replacements and disequilibrium textures. Deformation after crystallization can produce patchy zoning, cellular texture, among others [17] giving rise to the traps to capture electrons-holes that are responsible for the luminescence emission.

The bulk chemical analysis of the sample is: SiO_2 50.33%, Al_2O_3 29.68%, K_2O 10.81, Li_2O 4.63%, F 2.78%, Rb_2O 0.96%, MnO 0.40%, Na_2O 0.17%, Fe_2O_3 (total) 0.10%, CaO 0.09%, P_2O_5 0.04%, TiO_2 0.01, Loss on Ignition 2.30%. The content of impurities (in ppm) is: Cs 4293, Ni 510, Sn 242, Ce 112, Sb 97, Zn 80, Mo 36, Pb 10, V 10, Co 7, Sr 4, Cr 1. The chemical composition was analyzed in different regions of the sample, showing a homogeneous composition. This result is in good agreement with the homogeneous structure and composition detected in the ESEM measurements.

Figure 2 shows the CL spectral emission of the lepidolite in the UV-IR region (from 200 to 900 nm). Taking into account both, mathematical (second derivatives the regression coefficient of fitting -r-) and the physical criteria, the spectrum was deconvoluted into seven wavebands. The experimental CL spectral data was fitted by a sum of seven multiparameter Gaussian functions using the Peak Fit program (supplied by Jandel Scientific Software, Erkrath, Germany). All the analyzed parameters (i.e. position in nm, energy in eV, FWHM in nm, relative integrated area and relative intensity of the peaks) were refined to a confidence limit of 95% accuracy (Table 1) where λ_{Max} is the

position of the maxima in nanometers; E_{Max} is the peak energy value in electron-volt; I_{Max} is the intensity of the maxima in percent; FWHM corresponds to the full-width at half maximum and A is the area of the peak in percentage. These data have been estimated from the experimental curves (Fig 2), where the solid lines correspond to the calculated fitted gaussian peaks, which make up the calculated fitted dashed line. This encircling line is directly compared with the experimental line that corresponds to the experimental curve for the CL luminescence spectra analysis. The deconvoluted CL fitted peaks are centered at 330, 397, 441, 489, 563, 700 and 769 nm.

UV peaks are associated with structural defects of the lattice. The 340 nm emission peak is very common in the luminescence spectra of silicates due to the lattice stress in their 3D framework silicon–oxygen structure [18]. These Si–O strained structures could include some non-bridging oxygen (NBOC) atoms or silicon vacancy-hole centers and Si–O bonding defects. Therefore, we can speculate that lepidolite structure includes such centers, which seem to be responsible for this common 330 nm emission. Many Si–O bonds undergo an additional stress due to different processes, namely dehydration or dehydroxylation or both, involving losses of H_2O, with hydrogen atoms bonded to the lattice, or the breaking of hydroxyl groups, also bonded to the silicate framework. Emission bands at 335 – 345 nm were attributed to the emission of intrinsic defects-distorted tetrahedral complexes SiO_4^{4-}, which could exist in two non-equivalent crystal positions [19]. According to Itoh and coworkers [20], the 397 nm emission can be attributed to $[AlO_4]^-$ centers, through electron-hole mechanisms [21]. Due to the exposure to the electron beam, the electrons are released from the oxygen atoms closed to the aluminum giving rise to electron-hole pairs. It should generate $[AlO_4/h^+]$ centers in which alkali atoms (Li^+) diffuse from the lattice away. The alkali should join to an electron (e) to become neutral in the crystal network. $[AlO_4/h^+]$ centers combined with electrons are the origin of the $[AlO_4]^o$ centers. At the same time, these centers can be linked to Li or electron-holes producing $[AlO_4/Li^+]$ and $[AlO_4/h^+]$ centers respectively. The production-annihilation of luminescent $[AlO_4]^o$ centers could be analyzed in terms of ionic self-diffusion. In this case the electron beam radiation should increase the ionicity of the Si-O bonds modifying the ground state where each Si atom has four valence electrons and each O atom six valence electrons, implying that O states would exceed in number Si states by 3:1 considering atoms widely separated. The resulting centers $[AlO_4/Li^+]$, $[AlO_4/h^+]$ and $[AlO_4]^o$ are formed during self-diffusion processes

through the bulk and interfaces due to changes in the temperature of the lattice [22, 23]. The band at 441 nm can be associated with radiation-induced defects, i. e. O^- color centers [24] in agreement with EPR (electron paramagnetic resonance) spectroscopy results [25]. Bands between 470 and 500 nm have been associated with $[AlO_4]^o$ centers [26]. The green band at 563 nm, which is common in strain-free aluminosilicates, can be attributed to Mn^{2+}. According to Garcia-Guinea and co workers [27], Mn^{2+} replaces calcium in their lattice sites. However, this broad emission band can be attributed to Mn^{2+} in Li sites [28], or in Al sites or in both [29]. According with Krbetschek et al. [26] the CL emission between 700 and 780 nm could be associated with the presence of Fe^{3+} cations.

Fig. 3a shows the changes in the UV-blue TL glow curves of non-irradiated samples (NTL) after different preheating in a range from 275°C to 460°C. The natural TL glow curve consists of a low intense broad peak centred at 330°C moving continuously towards higher temperatures when preheating treatment (T_{stop}) ranges from 275°C in steps of 25-40°C. The maximum intensity and the peak area also decrease while the higher temperature region including a shoulder peaked at ca 500°C, remains practically unaffected. In Fig. 3b the prompt glow curve of a 1Gy irradiated sample (ITL) together with those obtained after different preheating in a range 75-130°C is shown. Prompt glow curve displays two maxima. The first one is a very narrow peak that appears at 100°C and fades very quickly because of the thermal treatment. This highly unstable peak is associated to the shallowest traps that become emptied in preheated samples, being therefore useless for dosimetric purposes. The second one, a low intense broad peak, is centred at 180°C and its behaviour should correspond to a continuous trap distribution similar to the non-irradiated lepidolite, as well as those other mineral (i.e. Na rich feldspars, albite [30] or K-rich feldspars, microcline [31]) and polymineral materials (meteorites [32]). This assumption is supported since both NTL and ITL glow curves display compound glow curves with a trap structure that cannot be explained employing the commonly accepted model based on the discrete trap distribution model because it was not possible to determine some physical parameters such as trap-energies or pre-exponential factors after being analyzed in terms of both first (corresponding to the cases where the intensity of the TL is proportional to the concentration of thermally released charges) and second order kinetics equations (where the thermally released charges are retrapped at least once before the recombination process). The best fitting

parameters obtained, based on the value of the factor of merit, were unsatisfactory. Therefore, due to this complexity of the TL glow curves one could assume a structure of a continuous trap distribution involving multiorder kinetics. Consequently, there is the typical shift of the maximum peak towards higher temperatures and a change in the shape and intensity of the TL distribution depending on thermal pre-treatment that could engage consecutive breaking and linking of bonds of Al-O, Fe-O including dehydroxylation and redox reactions in the material.

Table 2 shows the activation energy, *E*, calculated for both, natural (non-irradiated) lepidolite preheated at different temperatures (T_{stop}) in the range 275 - 460 °C, and 1 Gy irradiated samples preheated in the range 75 – 130 °C by means of the initial rise (IR) method [33]. In both cases, the maximum moves towards higher energies when increasing the annealing temperature due to the emptying of these traps. The natural sample pre-heated at 380°C was no possible to fit with the initial rise (IR) criterion due to the influence of two components in the TL glow curve. The IR method [34] is based on the hypothesis that occupancies of the relevant states remain almost constant for the lowest temperature side of the TL peak and, consequently, this side of the peak will follow an exponential dependence regardless of the kinetic order and the applicability of the quasi-equilibrium approximation $I_{TL} \alpha \exp(-E/kT)$, where I_{TL} is the TL intensity, k is the Boltzmann´s constant and T is the temperature. Therefore, in the Arrhenius plot ($\ln I_{TL}$ vs 1/T), the activation energy E can be obtained from the slope –E/k, irrespectively of any other kinetic parameter. Fig. 4 displays the Arrhenius plot of the low-T side of the natural and 1 Gy irradiated TL UV-blue emission of the no-preheated samples with the experimental data market on the fitting line. The activation energy for the natural (non-irradiated) and 1 Gy irradiated samples is 1.27 and 0.52 eV, respectively. The estimated value of correlation coefficient (*r*) is 0.997 in both cases, indicating a good fitting.

4. Conclusions

Luminescence properties of lepidolite have been scarcely studied. The investigated lepidolite, collected from Mangualde (Portugal) shows homogeneous chemical composition in agreement with the homogeneous structure observed by the ESEM technique. The deconvolution of the CL emission shows seven peaks centered at 330,

397, 441, 489, 563, 700 and 769 nm related with the presence of point defects associates with Mn^{2+} and Fe^{3+} or structural defects, i.e. non-bridging oxygen hole centers or $[AlO_4]$ centers. The maximum peak of the TL glow curves of non-irradiated and 1Gy irradiated samples shift towards higher temperatures and change in shape and intensity depending on thermal pre-treatment that could engage consecutive breaking and linking of bonds of Al-O, Fe-O including dehydroxylation and redox reactions in the material. For the natural (non-irradiated) lepidolite preheated at different temperatures in the range 275-460 °C, and 1 Gy irradiated samples preheated in the range 75–130 °C, the maximum moves towards higher energies when increasing the annealing temperature due to the emptying of these traps. The activation energy calculated by means of the initial rise (IR) method is 1.27 and 0.52 eV for both samples, respectively. In each case, the Arrhenius plot shows a very good correlation coefficient. Luminescence properties of lepidolite allow us to think the potential use of this material, for instance, in the field of retrospective dosimetry; nevertheless further works is necessary to confirm such assertion.

Acknowledgments

This work was partially supported by the project CGL2010-17108. Y. Rodríguez-Lazcano also acknowledges financial support from the Council for Advanced Studies Program (JAE-Doc-CSIC, in spanish).

References

[1] J. L. Muñiz, V. Correcher, A. Delgado, Radiat. Prot. Dosim. 85 (1999) 63 – 66.

[2] W. H. Zhuo, W. Q. Liu, G. Huang, G. Y. Zhu, G. C. Ma, Nucl. Sci. Technol. 18 (2007) 362 – 365.

[3] T. Yagi, K. Kondo, T. Misawa, K. Ochiai, S. Ohnishi, K. Takakura, S. Sato, C. Konno, C. H. Pyeon, S. Shiroya, J. Nucl. Sci. Technol. 48 (2011) 777 – 785.

[4] Z. P. Yan, S. Cai, L. J. Miao, X. Zhou, Y. M. Zhao, J. Alloy Compd. 511 (2012) 101 – 106.

[5] M. R. Saeri, A. Barzegar, H. A. Moghadam, Ceram Int 37 (2011) 3083 – 3087.

[6] M. Rieder, J. Hybler, L. Smrcok, Z. Weiss, Eur. J. Mineral. 8 (1996) 1241 – 1248.

[7] V. Correcher, J. Garcia-Guinea, J. Lumin. 93 (2001) 303–312.

[8] V. Correcher, J. Garcia-Guinea, E. Crespo-Feo, Y. Rodriguez-Lazcano, P. Prado-Herrero, Thermochim. Acta 503–504 (2010) 12–15.

[9] P. R. Gonzalez, C. Furetta, B. E. Calvo, M. I. Gaso, E. Cruz-Zaragoza, Nucl. Instr. and Meth. in Phys. Res. B 260 (2007) 685–692.

[10] J. L. Bárcena, M. Urbina, A. P. Rowlands, P. Benitez, A. Millán, T. Calderón, Radiat. Prot. Dosim. 84 (1999) 289-292.

[11] N. Kristianpoller, Y. Kirsh, S. Shoval, D. Weiss, R. Chen, Nucl Tracks Radiat Meas 14 (1988) 101–104.

[12] M. Kasuya, T. Sakai, S. Takahashi, T. Hashimoto, Nucl Tracks Radiat Meas 16 (1989) 283–286.

[13] S. W. S. McKeever, Thermoluminescence of solids, Cambridge Univ. Press, New York, 1985.

[14] L. Bøtter-Jensen, G.A.T. Duller, Nucl. Tracks Radiat. Meas. Part D. 20 (1992) 549-553.

[15] V. Correcher, A. Delgado, Radiat. Meas. 29 (1998) 411-414.

[16] J. Garcia-Guinea, V. Correcher, Spectrosc. Lett. 33 (2000) 103-113.

[17] E. Roda, P. Keller, A. Pesquera, F. Fontan, Mineral. Mag. 71 (2007) 41 – 62.

[18] J. Garcia-Guinea, V. Correcher, L. Sanchez-Muñoz, A. A. Finch, D. E. Hole, P. D. Townsend, Nucl. Instrum. Meth. A 580 (2007) 648-651.

[19] E. I. Lipatov, V. M. Orlovskii, V. F. Tarasenko, V. I. Solomonov, J. Lum. 126 (2007) 817-821.

[20] N. Itoh, D. Stoneham, A. M. Stoneham, J. Appl. Phys. 92 (2002) 5036-5044.

[21] M. Martini, A. Paleari, G. Spinolo, A. Vedda, Phys. Rev. B 52 (1995) 138-142 .

[22] V. Correcher, J. M. Gomez-Ros, J. Garcia-Guinea, E. Crespo-Feo, Mater. Chem. Phys. 116 (2009) 143-147.

[23] V. Correcher, Y. Rodriguez-Lazcano, J. Garcia-Guinea, E. Crespo-Feo, Brazilian J. Phys. 40 (2010) 348-352.

[24] L. Sanchez-Muñoz, V. Correcher, J. Garcia-Guinea, A. Delgado, Nucl. Instrum. Meth. A 580 (2007) 679-682.

[25] B. Speit, G. Lehmann, J. Lum. 27 (1982) 127-136.

[26] M. R. Krbetschek, J. Goetzes, A. Dietrich, T. Trautmann, Radiat Meas 27 (1997) 695-748.

[27] J. Garcia-Guinea, V. Correcher, E. Rodriguez-Badiola, Analyst 126 (2001) 911 – 916.

[28] G. Walker, A. El Jaer, R. Sherlock, T. J. Glynn, M. Czaja, Z. Mazurak, J. Lum. 72 – 74 (1997) 278 – 280.

[29] R. K. Chandrasekhar, W. B. White, Phys. Chem. Minerals 18 (1992) 433 – 440.

[30] V. Correcher, J. M. Gomez-Ros, A. Delgado, Radiat. Prot. Dosim. 84 (1999) 547-549.

[31] V. Correcher, J. M. Gomez-Ros, J. Garcia-Guinea, Radiat. Meas. 38 (2004) 689-693.

[32] V. Correcher, L. Sanchez-Munoz, J. Garcia-Guinea, A. Delgado, Nucl. Instrum. Meth. A 580 (2007) 637-640.

[33] V. Correcher, J. M. Gomez-Ros, J. Garcia-Guinea, M. Lis, L. Sanchez-Muñoz, Radiat Meas. 43 (2008) 269-272.

[34] R. Chen, S.W.S. McKeever, Theory of Thermoluminescence and Related Phenomena. World Scientific Publishing, Singapore, 1997.

Figure captions:

Fig 1. ESEM (a) cross-sectional and (b) top view image of two pieces of the lepidolite sample.

Fig. 2. UV-IR CL spectral emission of the lepidolite fitted with seven multiparameter Gaussian functions. The solid lines correspond to the calculated fitted Gaussian peaks, which make up the calculated fitted dashed line.

Fig 3. (a) TL glow curves of non-irradiated lepidolite samples after different preheating in a range 275-460^{o}C. (b) TL glow curves of 1Gy irradiated samples preheated in a range of 75-130^{o}C.

Fig. 4. Arrhenius plot of the low-T side of the (a) natural and (b) 1 Gy irradiated TL UV-blue emission of no-preheated lepidolite (experimental data are market on the fitting line).

Figure 1

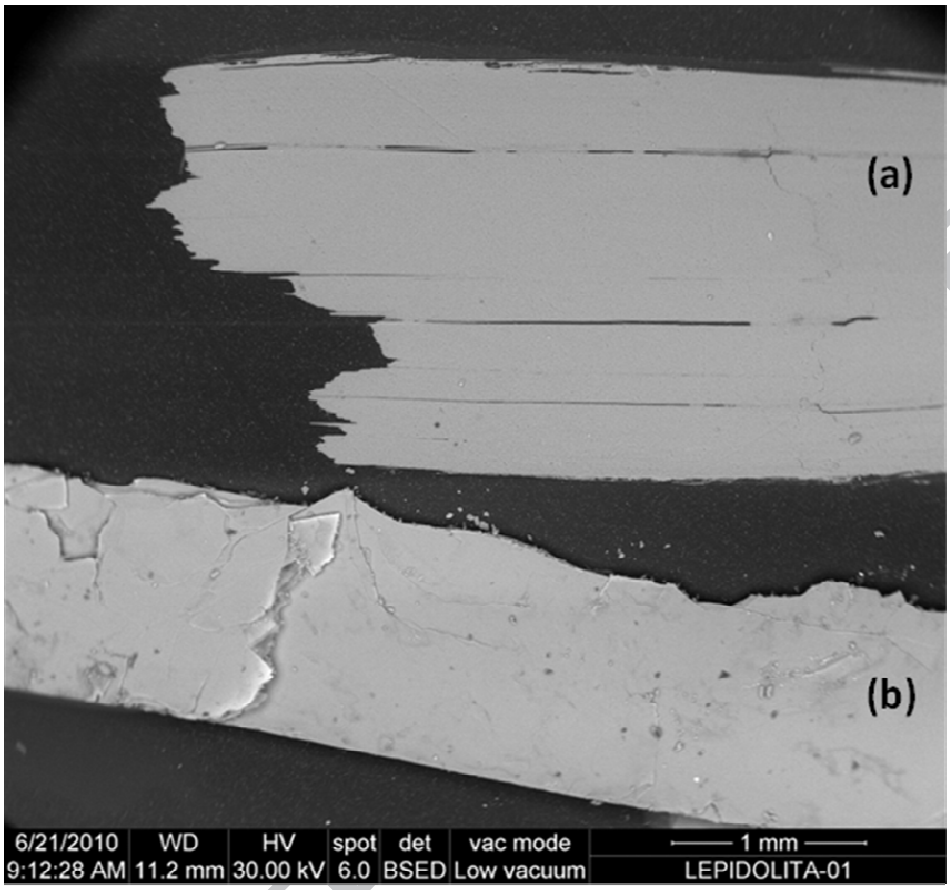

Figure 2

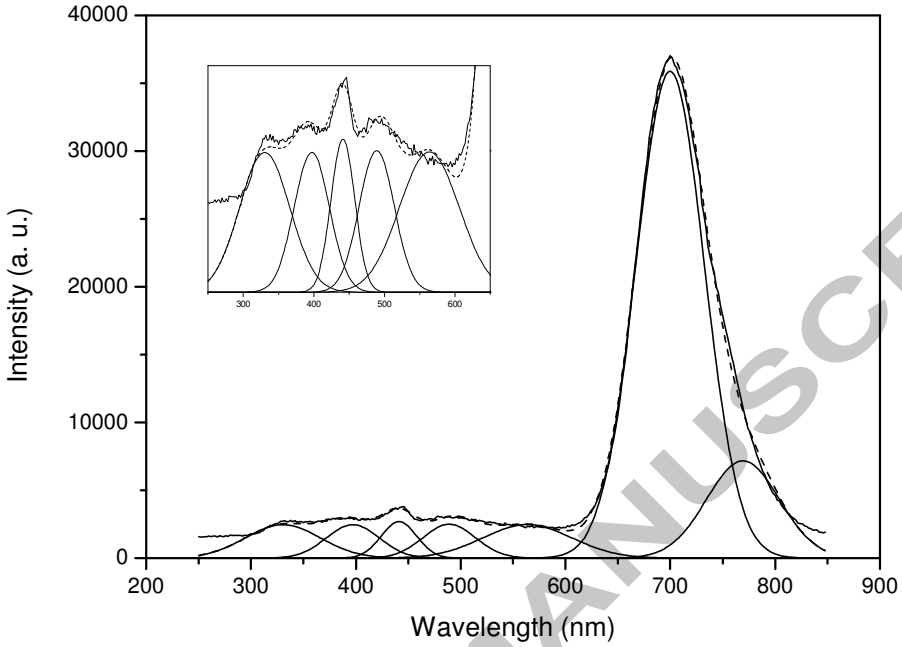

Figure 3a

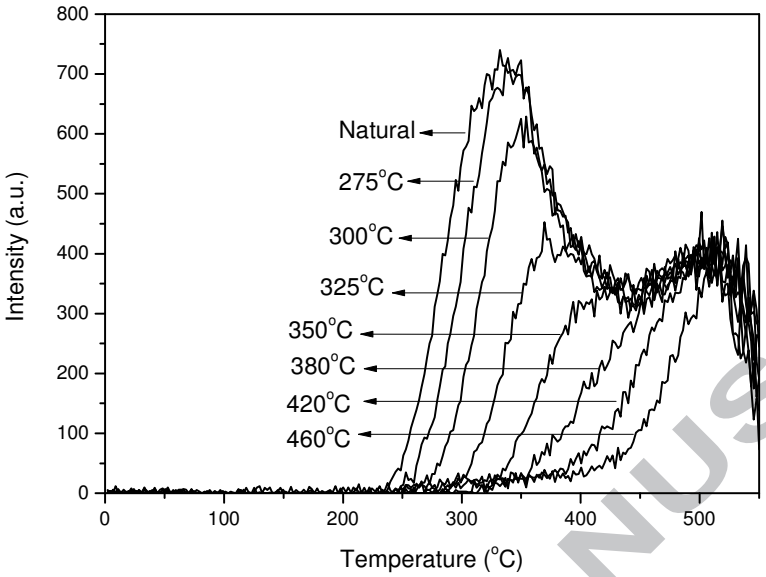

Figure 3b

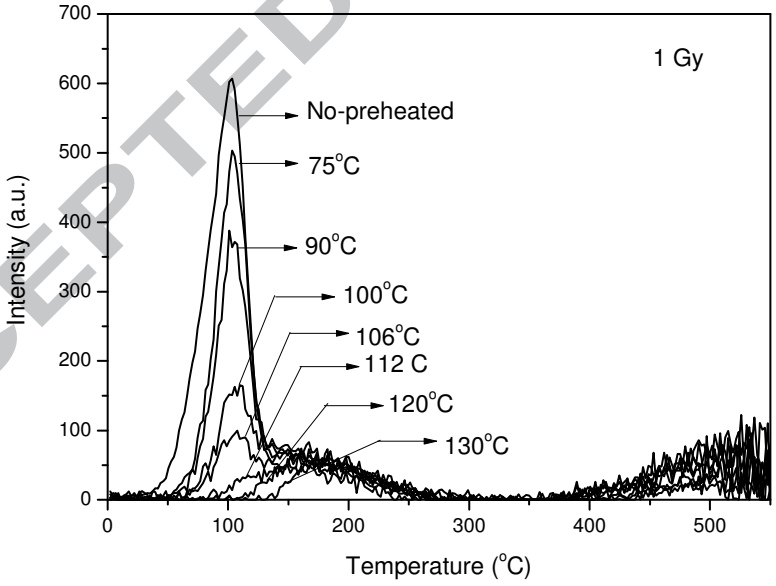

Figure 4a

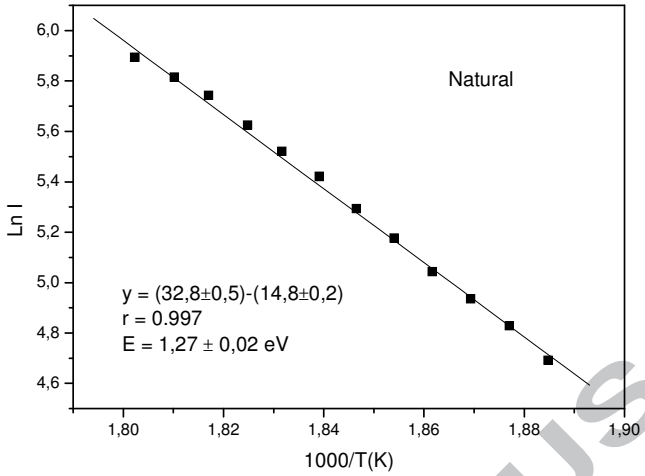

Figure 4b

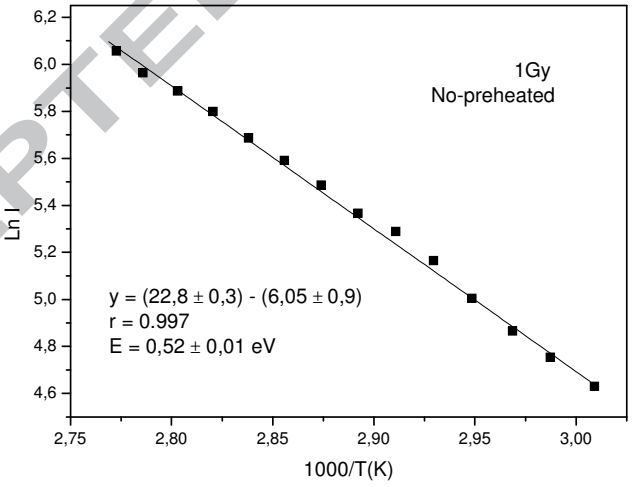

Table captions:

Table 1: Physical parameters obtained from the deconvolution into Gaussian peaks of CL emission of lepidolite (Fig 2) with $r^2 = 0.998$. All parameters were refined to a confidence limit of 95% accuracy.

Peak no.	λ_{Max} (nm)	E_{Max} (eV)	I_{Max} (%)	FWHM (nm)	A (%)
1	330	3.76	4.4	84	4.9
2	397	3.12	4.4	59	3.5
3	441	2.81	4.8	40	2.6
4	489	2.54	4.5	59	3.5
5	563	2.20	4.4	99	5.9
6	700	1.77	64.5	76	65.6
7	769	1.61	12.9	82	13.9

λ_{Max}: position of the maxima; E_{Max}: peak energy; I_{Max}: Intensity of the maxima; FWHM: full-width at half maximum, A: area of the peak. From Fig. 2.

Table 2. Calculation of the activation energy values by initial rise (IR) method resulting of the analysis of natural and induced TL glow curve of lepidolite.

Natural			Irradiated		
T_{stop}	IR range (^{o}C)	E (eV)	T_{stop}	IR range (^{o}C)	E (eV)
0	257-280	1.27(2)*	Prompt	53-88	0.52(1)
275	264-301	1.30(3)	75	81-92	0.71(3)
300	286-323	1.33(4)	90	77-99	0.76(3)
325	338-363	1.64(7)	100	80-95	0.77(5)
350	339-365	1.89(9)	106	75-98	0.84(8)
380	--	--			
420	412-473	1.01(3)			
460	445-496	1.18(4)			

* The number into parentheses is the uncertainties in the activation energy, *E*.

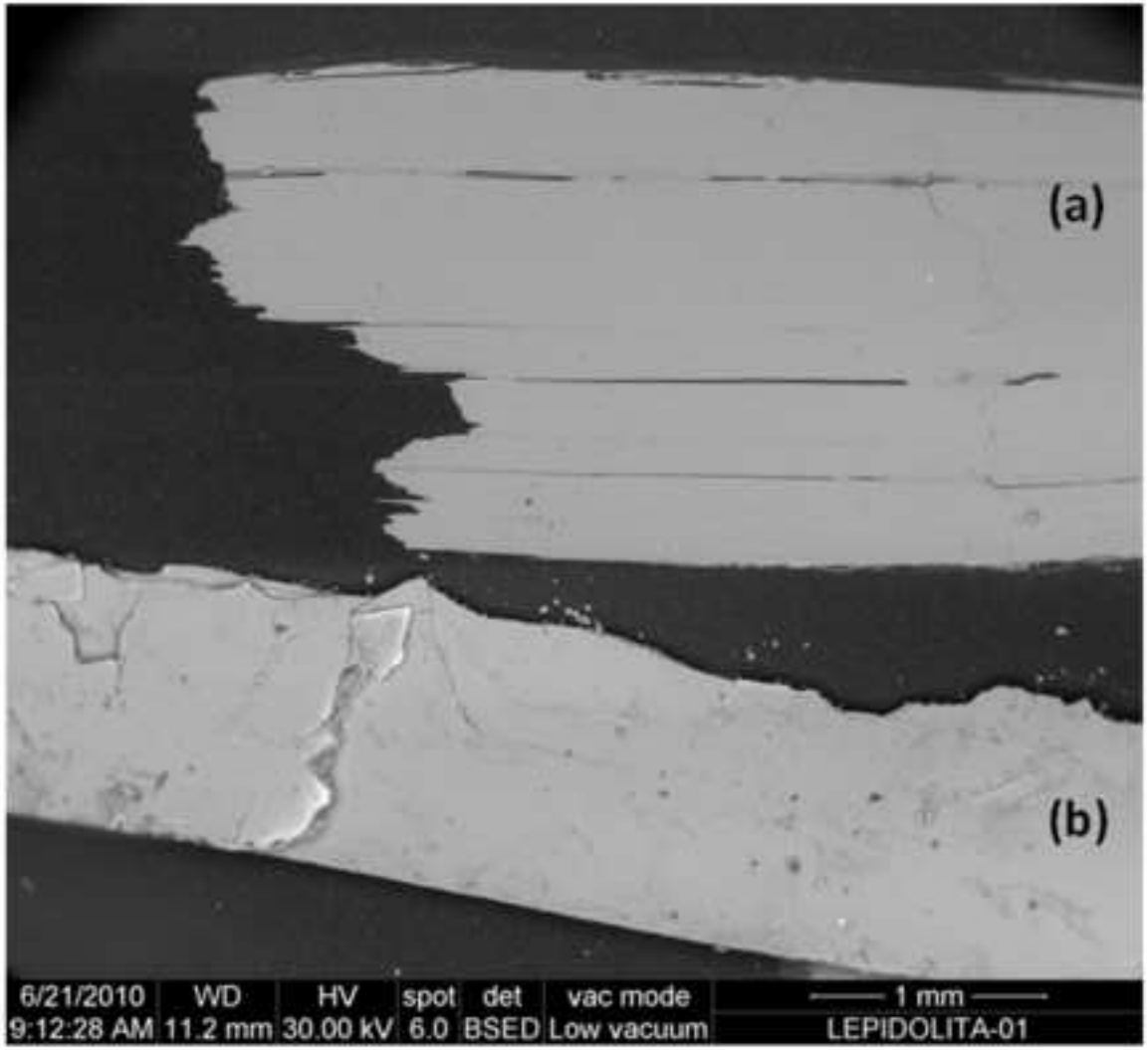

Research Highlights

- UV-IR CL shows seven peaks centered at 330, 397, 441, 489, 563, 700 and 769 nm
- CL bands are due to the presence of point defects and structural defects
- TL indicate a structure of a continuous trap distribution i. e. multiorder kinetics